Chemical Physics Letters 807 (2022) 140086

Contents lists available at ScienceDirect

Chemical Physics Letters

journal homepage: www.elsevier.com/locate/cplett

Experimental and theoretical investigation of electronic and optical properties of $CuAl_xGa_{1-x}Te_2$

A. Kassaa [a,b], N. Benslim [c], A. Otmani [a], L. Bechiri [c], A. Shankar [d], Abeer E. Aly [e,f,*]

[a] Departement of Physics, 20 August 1955 University Skikda, BP26, 21000 Skikda, Algeria
[b] Research Center in Industrial Technologies CRTI, P. O. Box 64, Cheraga 16014, Algiers, Algeria
[c] Department of Physics, Badji Mokhtar University Annaba, BP. 12, 23200 Annaba, Algeria
[d] Department of Physics, Kurseong College, Darjeeling 734203, India
[e] Department of Basic Science, Higher Institute of Engineering and Technology, Al Salam, Cairo, Egypt
[f] Department of Physics, Higher Institute of Engineering, El Shorouk Academy, Cairo, Egypt

ARTICLE INFO

Keywords:
$CuAl_xGa_{1-x}Te_2$
$CuGaTe_2$
Chalcopyrite
Solar cells
Density functional theory

ABSTRACT

The $CuAl_xGa_{1-x}Te_2$ powders used in this study were made by planetary ball milling the source element powders (Cu, Al, Ga and Te). All of the produced powders and thin films were polycrystalline, with a tetragonal chalcopyrite structure with (1 1 2) orientation, according to XRD analysis. The structural and electronic features of the $CuAl_xGa_{1-x}Te_2$ semiconductors were predicted using ab initio calculations based on Density Function Theory (DFT). The acquired results demonstrated that once the Al concentration increased, the lattice parameters and energy band gap changed in a way that was consistent with the experimental data.

1. Introduction

Due to its intriguing features and possible uses in nonlinear optical devices, photovoltaic solar cells, and light-emitting diodes, the I-III-VI_2 chalcopyrite semiconductor family (I = Cu, Ag; III = Al, Ga, In; VI = S, Se, Te) has received a lot of scientific attention [1,2]. Due to their high optical absorption coefficient (10^4 cm^{-1}) and tunable direct band gap [3,4] $CuInSe_2$ and $Cu(In,Ga)Se_2$ are frequently used as absorber materials in solar applications [5]. At the laboratory scale, $Cu(In,Ga)Se_2$ solar cells have recently attained a power conversion efficiency of 22.3% [6]. Due to their dependence on rare earth elements like In, Ga, and Se, these compounds have limitations that will be the principal barrier to their widespread application. Additionally, because to their improved moisture stability and distinctive optical properties, two-dimensional (2D) organic–inorganic perovskites have emerged as intriguing candidates for solar and photoelectric applications [7,8]. Despite having exceptionally better photovoltaic performance, these materials cannot be commercialised since the heavy metal lead they contain is hazardous to both living creatures and the environment [9,10].Researchers are concentrating on alternate absorber materials built from plentiful, environmentally benign precursors due to worries about Se toxicity and the lack of In in this material. $CuAl_xGa_{1-x}Te_2$, which is composed of nontoxic elements and is abundant in the earth's crust, can be thought of as a good replacement option for $Cu(In,Ga)Se_2$ in this situation. Particularly considering that this material may cover the ideal range of the solar spectrum thanks to its straight band gap, which ranges from 1.23 eV for $CuGaTe_2$ to 2.06 eV for $CuAlTe_2$ [11].Contrary to $Cu(In,Ga)Se_2$, the $CuAl_xGa_{1-x}Te_2$ material has sadly not received the attention from the scientific community that it merits despite having these excellent features. As a result, the fundamental physical characteristics of the substance are not entirely known. Only experimental research has been done on the material's massif and powder forms [12–14]. The most important fact is that no research has been done on the use of this substance as a thin film using any method. Investigating $CuAl_xGa_{1-x}Te_2$ as a thin film for solar cells is the aim of this study. Utilizing pre-synthesised $CuAl_xGa_{1-x}Te_2$ powders made by planetary ball milling as source materials, followed by vacuum thermal evaporation, $CuAl_xGa_{1-x}Te_2$ layers were formed on glass substrates. The influence of Aluminium content (x = 0, 0.2, 0.4, and 0.5) on the physical characteristics of the $CuAl_xGa_{1-x}Te_2$ powders and films was investigated using XRD, SEM, and XPS. Additionally, the structure, band structure, and density of states of $CuAl_xGa_{1-x}Te_2$ chalcopyrite materials with (x = 0, 0.5, and 1) have been calculated using the full potential linear augmented plane wave (FP-LAPW) approach. The WIEN2K code uses the density functional theory (DFT) to put this strategy into practice.

* Corresponding author at: Department of Basic Science, Higher Institute of Engineering and Technology, Al Salam, Cairo, Egypt.
E-mail address: abeerresmat782000@yahoo.com (A.E. Aly).

https://doi.org/10.1016/j.cplett.2022.140086
Received 4 June 2022; Received in revised form 19 September 2022; Accepted 24 September 2022
Available online 9 October 2022

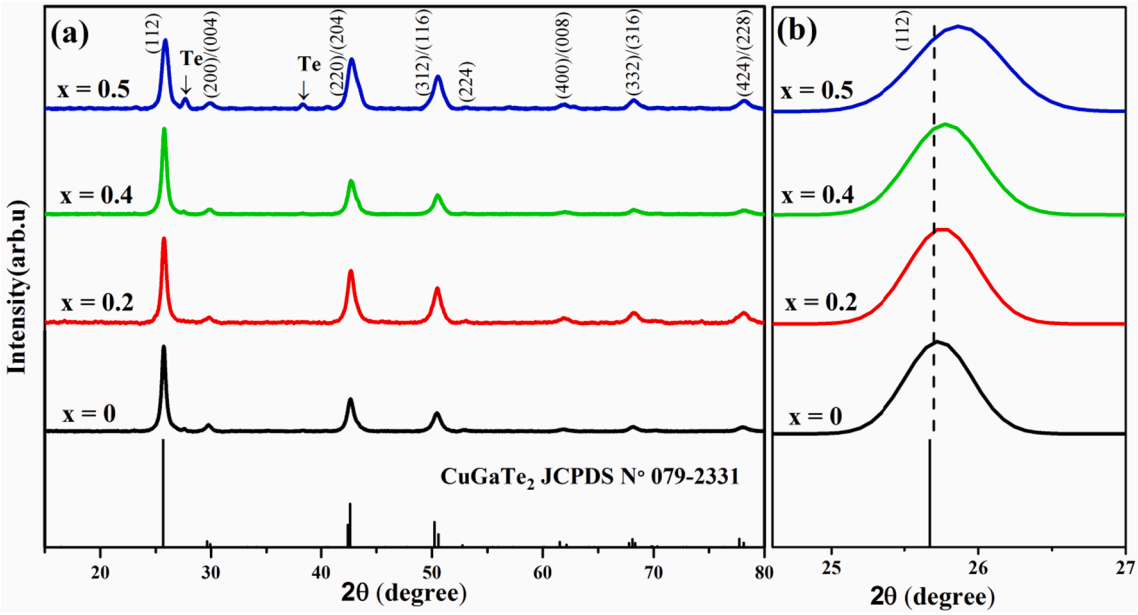

Fig. 1. **a** XRD patterns of $CuAl_xGa_{1-x}Te_2$ Powders, **b** (1 1 2) peak position shift with Al content.

Table 1
Structural parameters of $CuAl_xGa_{1-x}Te_2$ powders and thin films (x = 0, 0.2, 0.4 and 0.5).

x	powders					thin films				
	2θ (°)	d_{112} (Å)	*a* (Å)	*c* (Å)	*V*(Å^3)	*2θ* (°)	d_{112} (Å)	*a* (Å)	*c* (Å)	*V*(Å^3)
0	25.718	3.461	5.993	11.997	430.92	25.720	3.460	5.978	12.054	430.81
0.2	25.758	3.455	5.984	11.976	428.88	25.846	3.444	5.947	12.006	424.66
0.4	25.817	3.448	5.976	11.929	426.01	25.957	3.429	5.917	11.977	419.35
0.5	25.868	3.441	5.971	11.877	423.54	26.045	3.418	5.901	11.920	415.18

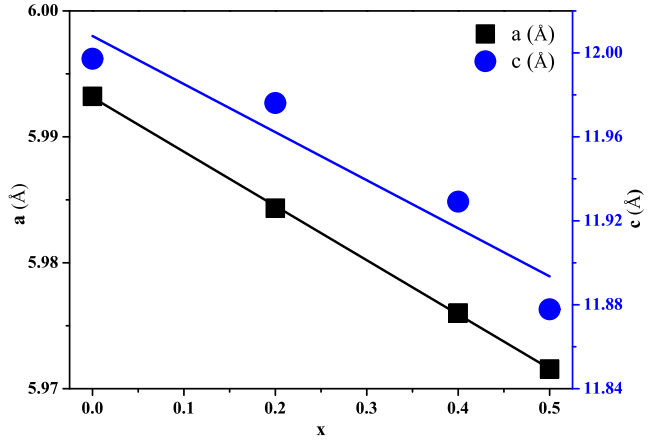

Fig. 2. Lattice parameters *a* and *c* of $CuAl_xGa_{1-x}Te_2$ powders (x = 0, 0.2, 0.4 and 0.5).

2. Experimental and computational details

2.1. Experimental procedures

Mechanical alloying was used to create nanostructured $CuAl_xGa_{1-x}Te_2$ powders with (x = 0, 0.2, 0.4, and 0.5). Cu, Ga, Al, and Te powders with high purity of 99.99 % were packed in a cylindrical steel tank under a pure argon gas atmosphere in a planetary ball mill (Fritsch Pulverisette7). The milling operation was carried out at a rotational speed of 200 rpm, with a mass ratio of 6:1 of balls to powders and a 3 h milling period. $CuAl_xGa_{1-x}Te_2$ thin films were made by evaporating their milled powders on glass substrates. The films were deposited using BALZERS high vacuum deposition equipment at a substrate temperature of roughly 300 °C and a vacuum of 2.10^{-5} torr. The structural properties of the generated powders and thin films were determined using a Philips-X 'Pert X-Ray diffractometer (XRD) with CuK radiation (=1.5406). The chemical compositions of the powders were studied using a Phenom-ProX scanning electron microscope (SEM). The chemical binding energy of the powders was measured using a Kratos-Axis Ultra X-ray photoelectron spectrometer (XPS) with AlK anode radiation (photon energy = 1486.6 eV). The optical properties of the deposited films were studied using a Shimadzu spectrophotometer to assess transmittance (UV–Vis-NIR).

2.2. Computational details

The ground-state properties of $CuAl_xGa_{1-x}Te_2$ alloys were studied using a quantum mechanical modeling technique based on an efficient semi-relativistic variant of the FP-LAPW method within the DFT. The modified Becke-Johnson exchange potential (mBJ) approach has been used to approximate the effects of electron exchange and correlation [15,16]. The space is composed of: (1) a non-overlapping Muffin tin (MT) sphere centred on the atomic sites, where the basis set is expanded as a linear combining of radial and spherical harmonic functions at the same time using the FP-LAPW method; (2) The plane wave is used to enlarge the basis set in an interstitial region (IR) between the MT spheres. The convergence conditions were set to 8 (the R_{MT} * *Kmax* cut-off value), where R_{MT} and *Kmax* are the minimum radius of the muffin tin sphere and the highest value of the plane wave vector, respectively (K). Different values of RMT were used in the calculation, namely 2.3,

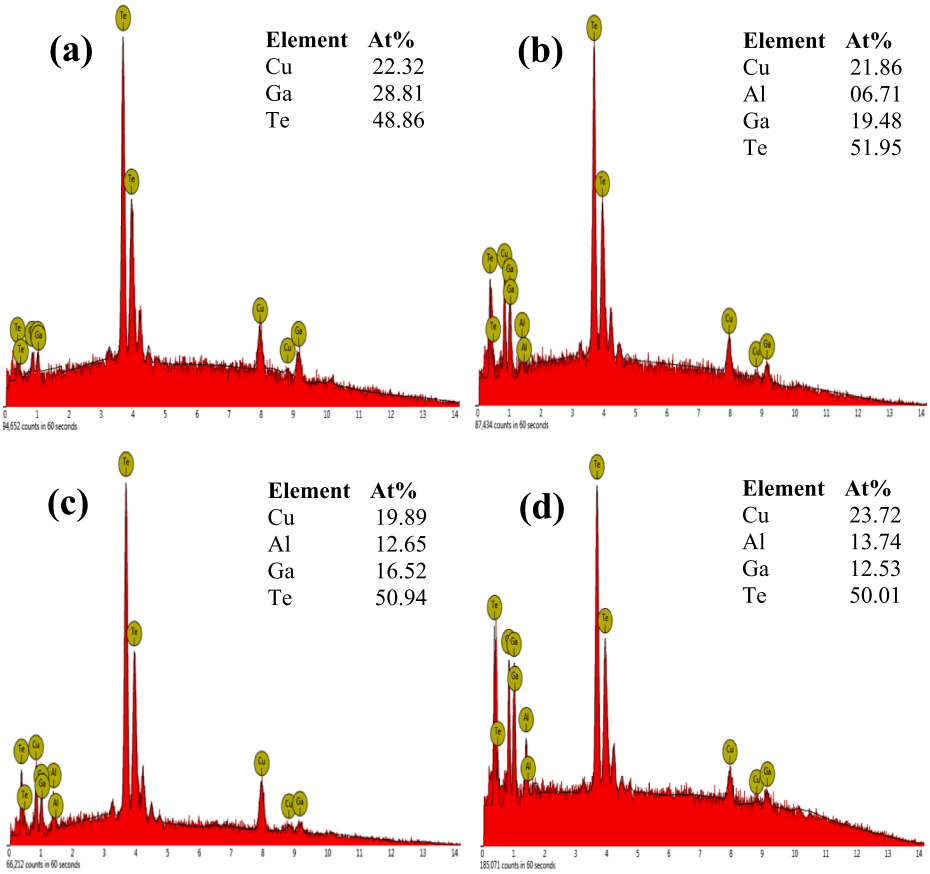

Fig. 3. EDX spectra of $CuAl_xGa_{1-x}Te_2$ powders **a** × = 0, **b** × = 0.2, **c** × = 0.4 and **d** x = 0.5.

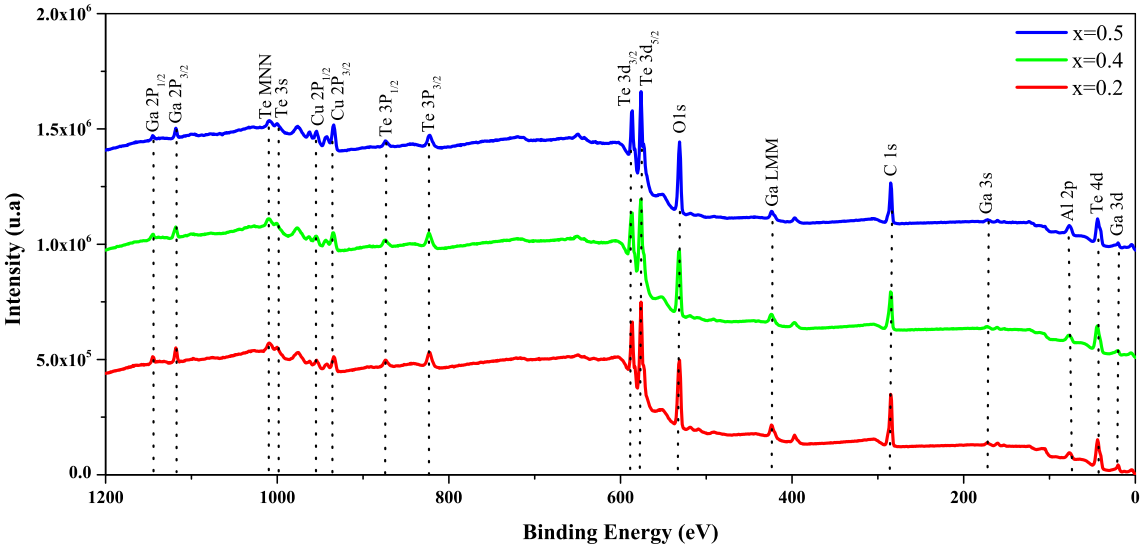

Fig. 4. Survey XPS spectrum of the $CuAl_xGa_{1-x}Te_2$ powders (x = 0.2, 0.4 and 0.5).

2.4, 1.8, and 3.2, based on the size of the constituent atoms Cu, Ga, Al, and Te, respectively. In the MT sphere and the IR, the maximum values of *lmax* = 14 and *Gmax* = 13 were chosen for the potential and no spherical contribution to the charge density, respectively. The Brillouin zone (BZ) integration was performed with a grid of 17*17*17 dense k-points created automatically using the Monkhorst and Pack convention and a 10^{-4} Ry energy convergence criterion [17].

3. Results and discussion

3.1. Structural analysis of $CuAl_xGa_{1-x}Te_2$ powders

$CuAl_xGa_{1-x}Te_2$ (x = 0, 0.2, 0.4, and 0.5) X-ray powder diffraction patterns are shown in Fig. 1. Since there is no standard JCPDS file for $CuAl_xGa_{1-x}Te_2$, the $CuGaTe_2$ standard was used to identify the formation of $CuAl_xGa_{1-x}Te_2$. When x = 0, the main observed peaks can be

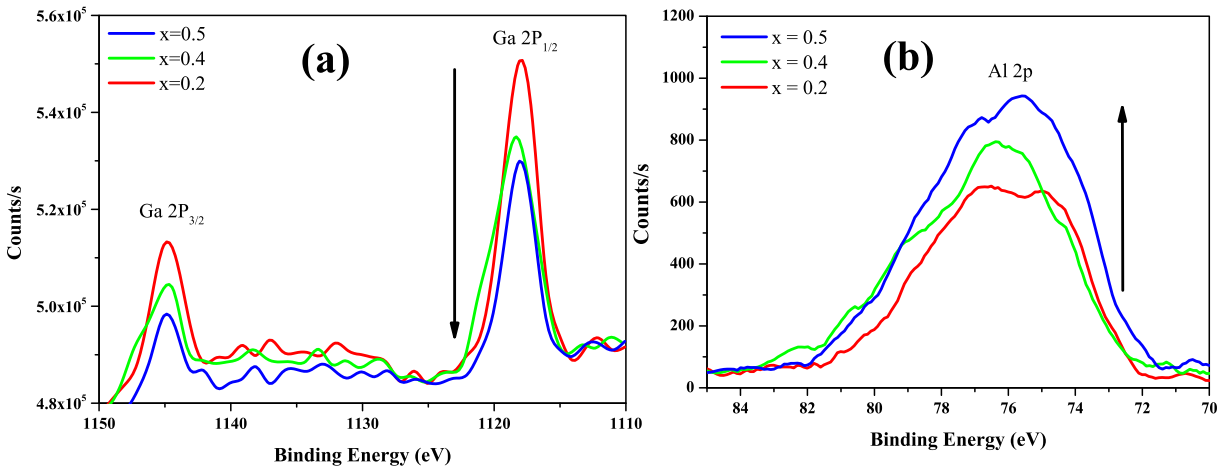

Fig. 5. High-resolution scans of **a** Ga3d, **b** Al2p for $CuAl_xGa_{1-x}Te_2$ powders (x = 0.2, 0.4, and 0.5).

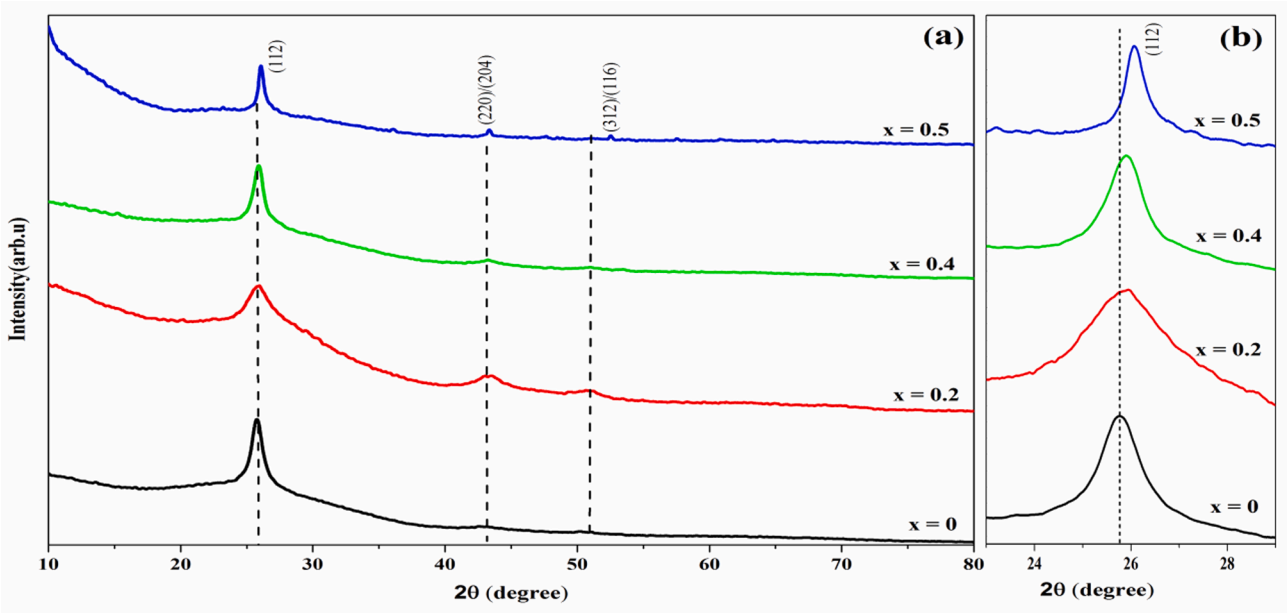

Fig. 6. **a** XRD patterns of $CuAl_xGa_{1-x}Te_2$ thin films, **b** (1 1 2) peak position shift with Al content.

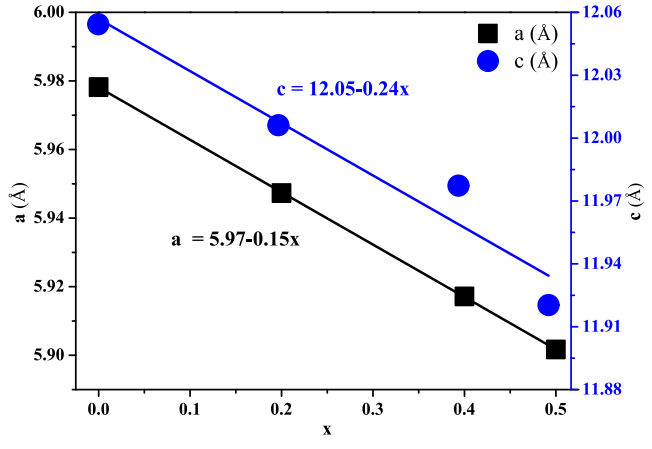

Fig. 7. Lattice parameters *a* and *c* of $CuAl_xGa_{1-x}Te_2$ thin films (x = 0, 0.2, 0.4 and 0.5).

attributed to the $CuGaTe_2$ phase (JCPDS N°. 079-2331), which belongs to the chalcopyrite family, as seen in Fig. 1a. The principal diffraction peaks of tetragonal chalcopyrite were indexed as (1 1 2), (2 0 0)/(0 0 4), (2 2 0)/(2 0 4), (3 1 2)/(1 1 6), (4 0 0)/(0 0 8), (3 3 2)/(3 1 6), and (4 2 4)/(2 2 8), with (1 1 2) being the preferred crystallographic orientation. When comparing the diffractograms of the various compounds, it was discovered that all samples had two small diffraction peaks at (2 = 27.62° and 38.36°, respectively). These peaks are very similar to those of Te (JCPDS N° 01-0727). Referring to Fig. 1b, the (1 1 2) peak reflection shifted to a higher angles with increasing Al content, which can be explained by the decrease of the lattice spacing d_{112} (Table 1). Several writers have reported this divergence from Vegard's law for $CuAl_x$-$Ga_{1-x}Te_2$ powders in various chalcopyrite materials [12,18–20]. Using the Scherrer formula [21], the average crystallite size (D) of all samples is calculated from the most intense peak (1 1 2). The calculated average crystallite sizes of the $CuGaTe_2$, $CuAl_{0.2}Ga_{0.8}Te_2$, $CuAl_{0.4}Ga_{0.6}Te_2$ and $CuAl_{0.5}Ga_{0.5}Te_2$ compounds are 18.3 nm, 14.4 nm, 12.4 nm and 11.5 nm, respectively. These findings show that when the Al content increased, the crystallite size shrank. The Bragg equation was used to determine the lattice parameters (*a, c*) of $CuAl_xGa_{1-x}Te_2$ powders from

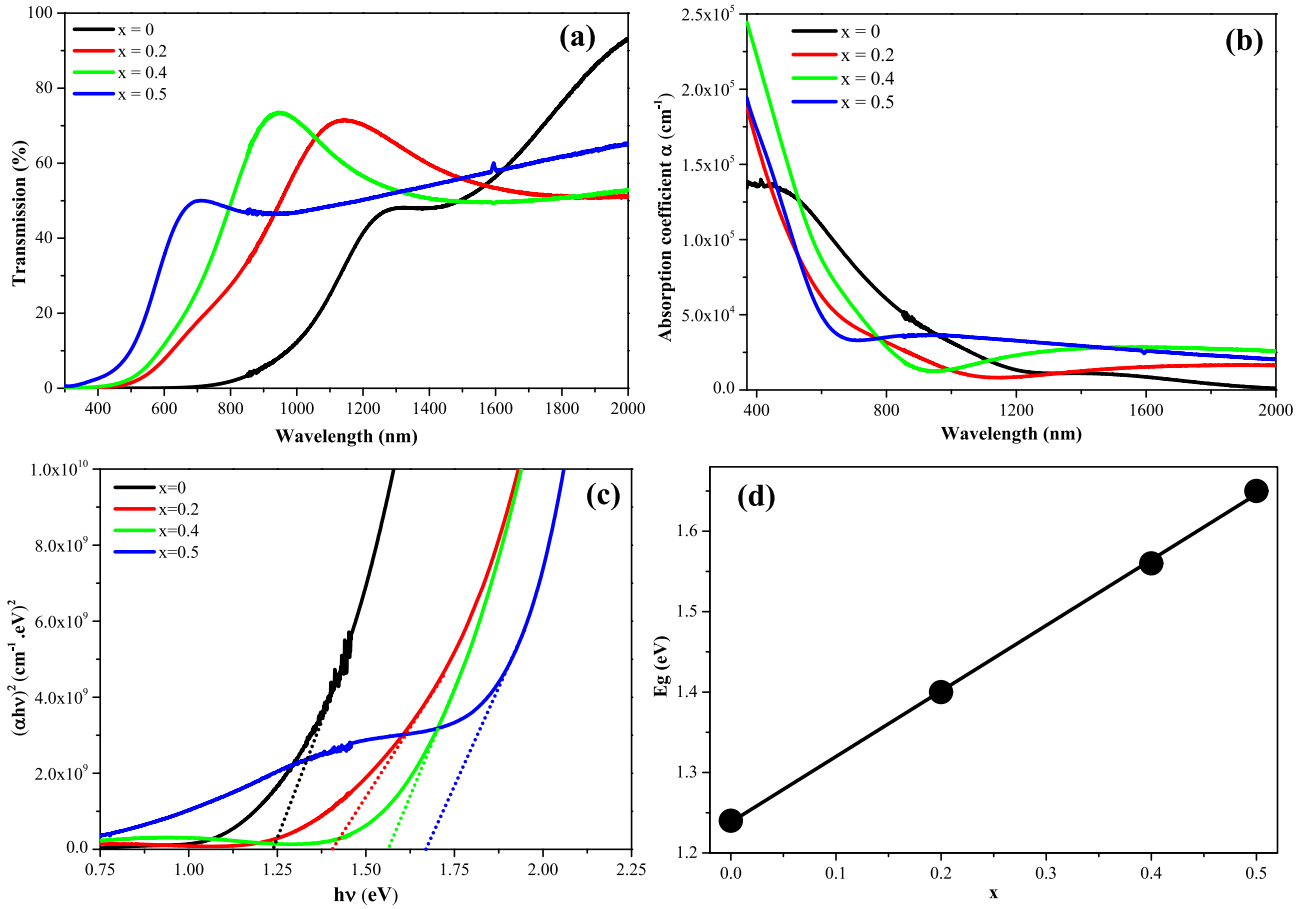

Fig. 8. **a** Transmittance spectra of $CuAl_xGa_{1-x}Te_2$ thin films, **b** Absorption coefficient versus wavelength, **c** Plot $(\alpha h\nu)^2$ versus $(h\nu)$, and **d** The band gap versus Al content (x).

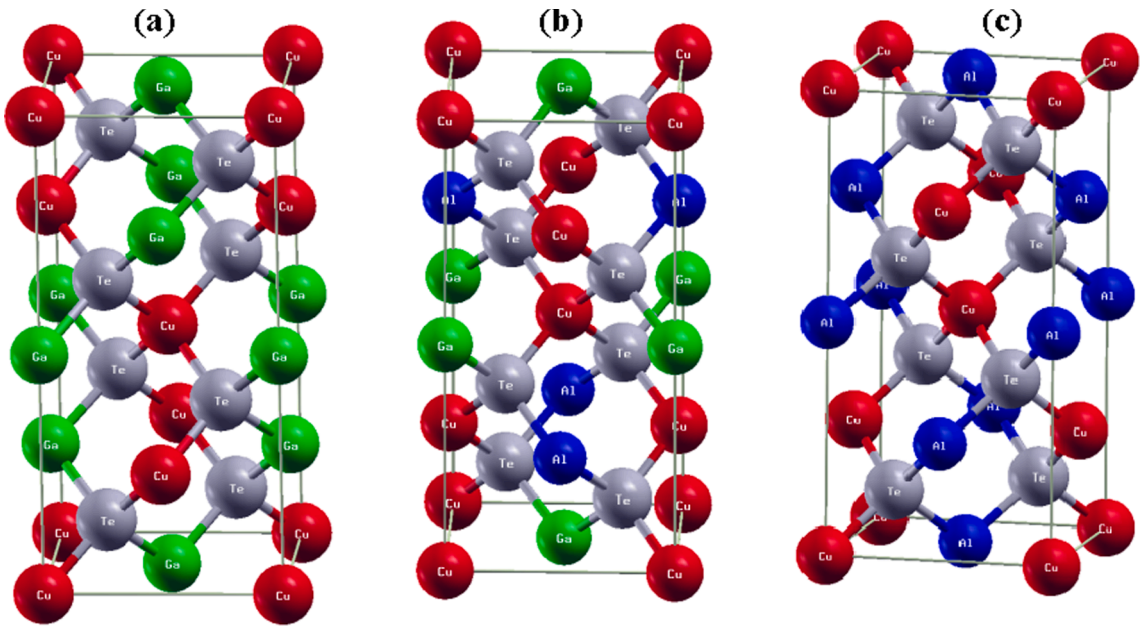

Fig. 9. Chalcopyrite structure of **a** $CuGaTe_2$, **b** $CuAl_{0.5}Ga_{0.5}Te_2$ and **c** $CuAlTe_2$.

the positions of the peaks corresponding to the (112) and (220) reflections. Table 1 summarises these figures. The values of *a* and *c* for pure $CuGaTe_2$ in this study are 5.9932 and 11.9972 Å, respectively, which differ somewhat from the values in JCPDS N° 079–2331 (a = 6.0235 and c = 11.9398 Å) and prior $CuGaTe_2$ composition studies [22,23]. Fig. 2 shows a plot of the lattice parameters *a* and *c* versus the

Table 2
The equilibrium lattice constant of $CuAl_xGa_{1-x}Te_2$.

$CuAl_xGa_{1-x}Te_2$	Lattice constant (Å)	Bulk modulus (GPa)	Bulk Pressure (GPa)	Internal parameter (u)	E_g (eV)
x = 0	a = b = 6.143 c = 12.608	51.665	6.7287	0.23639	1.073
x = 0.5	a = 6.025 c = 11.893	47.3829	4.2376	0.22736	1.24
x = 1	a = b = 5.904 c = 11.524	50.7832	5.2306	0.23952	2.0

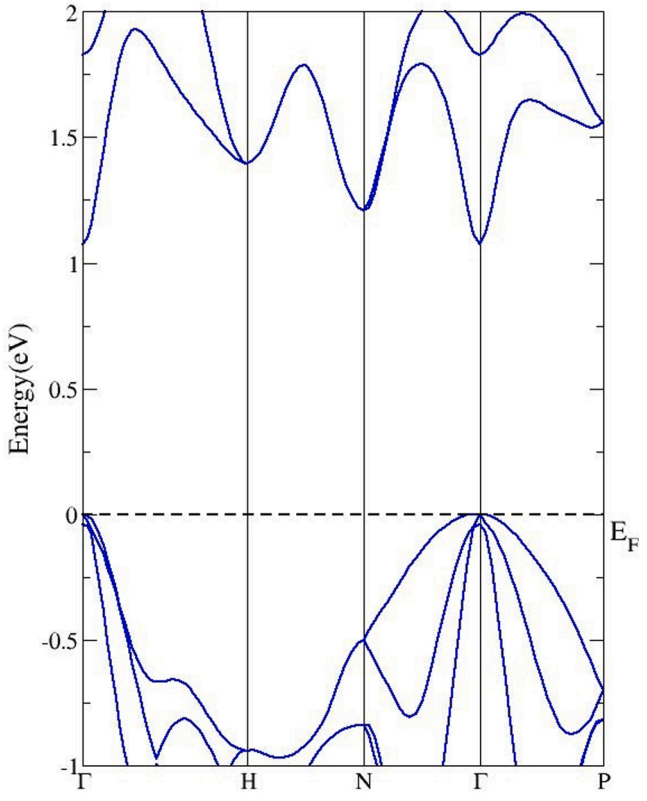

Fig. 10. Energy band structure of $CuGaTe_2$ using mBJ.

Al content variable x in $CuAl_xGa_{1-x}Te_2$ powders. As the x value grows, the values of *a* and *c* drop linearly. According to Vegard's law, the linear decrease in lattice parameters signals the creation of solid solutions, which is consistent with the literature [24]. The lattice contraction was produced by the replacement of Ga atoms (76.0 pm) by smaller Al atoms (67.5 pm) [25], resulting in a drop in *a* and *c* values. Similar results for $CuAl_xGa_{1-x}Se_2$ samples have been observed in the literature [12] and reported in other earlier publications [26–28].

3.2. Composition analysis of $CuAl_xGa_{1-x}Te_2$ powders

The chemical components (Cu, Al, Ga, and Te) of $CuAl_xGa_{1-x}Te_2$ powders are confirmed by the EDX spectrum shown in Fig. 3. At 9.5 keV, the relative intensity of the Ga peak decreases, which corresponds to the drop in Ga content. The relative intensity peak of Al at 1.5 keV, on the other hand, is increasing, with $CuAl_{0.5}Ga_{0.5}Te_2$ having the lowest intensity. The atomic percentages of elements in the produced powders, as well as the composition of near-stoichiometric and stoichiometric $CuAl_xGa_{1-x}Te_2$ powders, are confirmed by EDX quantitative data. In the same circumstances, the powders are copper-deficient but tellurium-rich.

3.3. XPS analysis of $CuAl_xGa_{1-x}Te_2$ powders

An XPS survey spectrum of $CuAl_xGa_{1-x}Te_2$ powders (x = 0.2, 0.4, and 0.5) is shown in Fig. 4. The Cu, Al, Ga, and Te peaks are all visible in the spectrums, regardless of the C 1 s and O 1 s peaks. The presence of C could be owing to environmental pollution, but the presence of O is most likely due to oxide development on the surface. It also displays the peak positions of the $Cu2p_{3/2}$, $Cu2p_{1/2}$ and Al2p and $Ga2p_{3/2}$, $Ga2p_{1/2}$ and $Te3d_{5/2}$, $Te3d_{3/2}$ levels of 933 eV, 953 eV and 76 eV and 1118 eV, 1144 eV and 575 eV, 586 eV, respectively. These findings are consistent with those reported for the $CuAl_{0.5}Ga_{0.5}Te_2$ sample by [13]. As can be seen in Fig. 5a, the content of the Ga element drops as the Al content increases, suggesting that Al atoms may successfully replace Ga atoms.

3.4. Structural analysis of $CuAl_xGa_{1-x}Te_2$ thin films

Fig. 6a shows the X-ray diffraction spectrum of $CuAl_xGa_{1-x}Te_2$ thin films (x = 0, 0.2, 0.4, and 0.5). For all films, the spectra revealed planes (1 1 2), (220/204), and (116/312) attributable to the chalcopyrite (tetragonal) structure, with no secondary phases formed. The chalcopyrite $CuGaTe_2$ (JCPDS N° 079-2331) was found to have three diffraction peaks that matched. The (1 1 2) diffraction peaks move to higher angles as the Al content increases, as seen in Fig. 6b, implying that the Ga sites in $CuGaTe_2$ were substituted by some smaller Al atoms, causing the lattice contraction. Table 1 shows the lattice characteristics, 2 pick position, and cell volume for $CuAl_xGa_{1-x}Te_2$. Fig. 7 shows a plot of the $CuAl_xGa_{1-x}Te_2$ films' lattice parameters *a* and *c* versus the Al content variable x. Vegard's law is rather well supported by the lattice parameters. These values are observed to decline linearly as the Al concentration increases, and can be represented as: $a = 5.97 - 0.15x$, $c = 12.05 - 0.24x$. The obtained lattice constants and cell volume of the $CuGaTe_2$ thin film are consistent with standard theoretical values and our $CuGaTe_2$ powder experimental results.

3.5. Optical properties

Fig. 8a shows the transmittance spectra of $CuAl_xGa_{1-x}Te_2$ thin films (x = 0, 0.2, 0.4, and 0.5). In the near-infrared band, the transmittance of the sample (x = 0) was found to be 93 %. The transmittance of the samples increases as the Al concentration in the visible and near-infrared spectrum increases. In the near-infrared wavelength band, the $CuAl_xGa_{1-x}Te_2$ films had transmittance values of roughly 70 %. The transmittance decays rapidly at 0 % in the visible wavelength region. Lambert's law [29] was used to get the absorption coefficient from this transmission data. Fig. 8b shows the absorption coefficient spectra of $CuAl_xGa_{1-x}Te_2$ films as a function of photon energy for various Al concentrations. In the visible band, all of the films show a moderately high absorption coefficient (>3.10^4 cm^{-1}), indicating that they are suitable for photovoltaic applications. The absorption coefficient values grow as the Aluminium content increases. The absorption coefficients for all wavelengths beyond 800 nm, on the other hand, become smaller and more steady. The optical band gap of $CuAl_xGa_{1-x}Te_2$ thin films has been estimated from the absorption spectrum using the following equation [30]: $(\alpha h\nu)^2 = A(h\nu - E_g)$, Where A is a constant, *h* is the Planck constant. As illustrated in Fig. 8c, the band gap (E_g) was calculated by plotting $(\alpha h\nu)^2$ versus photon energy ($h\nu$). The band gaps of $CuAl_xGa_{1-x}Te_2$ layers with × = 0, 0.2, 0.4, and 0.5 had E_g values of 1.23, 1.40, 1.56, and 1.65 eV, respectively. These results are consistent with prior $CuAl_xGa_{1-x}Te_2$ values reported [31]. In addition, the band gap value for $CuGaTe_2$ agrees well with the 1.23 eV value determined by

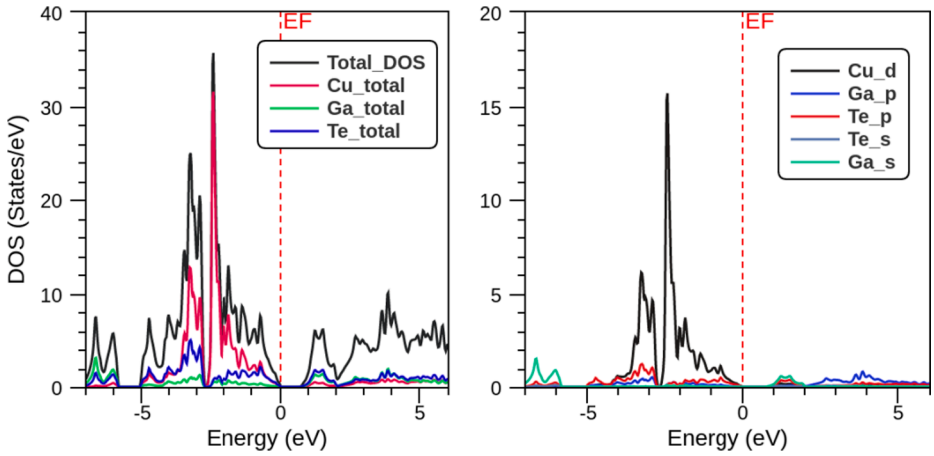

Fig. 11. Total and partial density of states for $CuGaTe_2$.

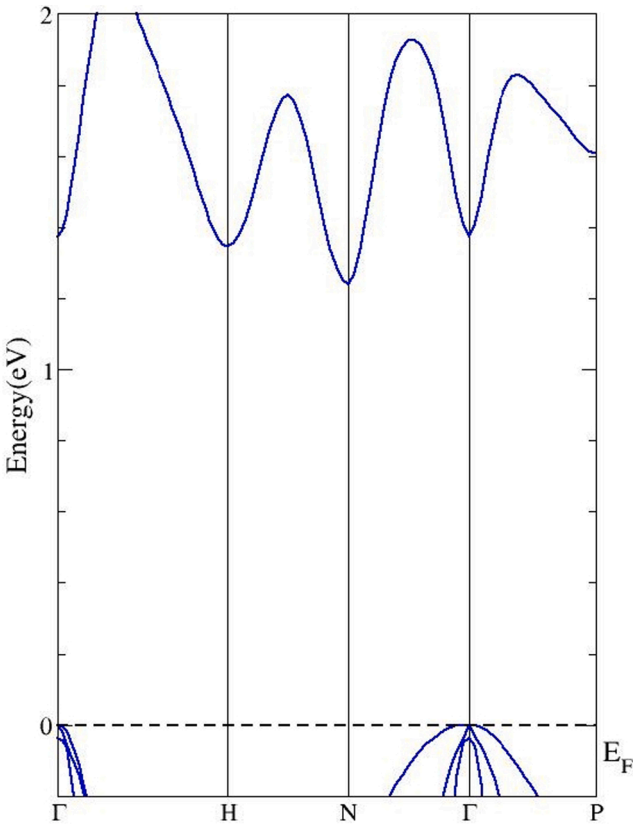

Fig. 12. Energy band structure of $CuGa_{0.5}Al_{0.5}Te_2$ using mBJ.

[32–34]. Fig. 8d demonstrates how the Al content affects the optical band gap of $CuAl_xGa_{1-x}Te_2$ layers. The band gap values of $CuAl_xGa_{1-x}Te_2$ layers are found to rise linearly with the Al concentration (see Fig. 9).

3.6. Computational results

3.6.1. Structural optimization

Cu(Al,Ga)Te_2 is a body-centered tetragonal chalcopyrite structure semiconductor with the space group I-42d (№ 122) [12]. The Cu atom is at the 4a (0 0 0) site, the Al/Ga atoms are at the 4b (0 0 1/2) site, and the Te atoms are at the 8d (u 1/4 1/8) site in the $CuAl_xGa_{1-x}Te_2$ (x = 0, 0.5, and 1) structure. The structural parameters of the ground state are obtained by minimising the total energy with respect to the unit cell volume. The equilibrium lattice constant of $CuAl_xGa_{1-x}Te_2$ was determined for various x (0, 0.5, and 1) compositions, as shown in Table 2. $CuGaTe_2$ optimization of unit cell volume leads to $a = b = 6.143$, $c = 12.608$ Å and $CuAlTe_2$ optimization of unit cell volume leads to $a = b = 5.904$, $c = 11.524$ Å, which is in good agreement with experimental [35] and theoretical results [36]. The unit cell of optimised $CuAl_xGa_{1-x}Te_2$ (x = 0, 0.5, and 1) structures is greatly shorter due to the substitution of big Ga atoms with smaller Al atoms, resulting in a drop in the lattice constant.

3.6.2. Electronic structure

The band structure of $CuAl_xGa_{1-x}Te_2$ (x = 0, 0.5, and 1) compounds is computed using the mBJ scheme based on the optimised structures. $CuGaTe_2$ band structure in high symmetry directions of the tetragonal Brillouin zone is shown in Fig. 10. The compound is a direct band gap semiconductor with an energy band gap of 1.073 eV because the valence band maximum (VBM) and conduction band minimum (CBM) are both located near the point of the Brillouin zone. The density of states (DOS) of $CuGaTe_2$ is depicted in Fig. 11, where it is clear that Cu-d states contribute the most to the valence bands, and that as energy moves away from the valence bands, these states cause the DOS to rise dramatically. Similarly, in the conduction band, the DOS does not climb as sharply as it does in the valence bands.

When compared to pure $CuGaTe_2$ with the VBM and CBM in the point of the Brillouin zone, the energy band gap increases to 1.24 eV with 50% Al incorporation in the Ga site, as shown in Fig. 12. Many earlier studies [37,38] have shown that the mBJ potential may produce highly precise energy band gaps while also being computationally efficient. When the compounds are treated with mBJ, a significant effect on the electronic band structures can be observed. We estimated the total density of states (TDOS) to characterise the nature of the electronic band structures, which is shown in Fig. 13. As can be observed from the DOS plot, the Te states contribute the most, while Ga and Al states contribute the least.

When the Ga atom is totally replaced by Al, the DOS and band structure show a similar pattern with an increase in the energy band value. Fig. 14 shows the $CuAlTe_2$ computed band graph. At the location, $CuAlTe_2$ has a straight band gap with VBM and CBM, and the obtained band gap is 2.0 eV. Our predicted band gap value is lower than the experimental value (2.06 eV) [39]. This type of underestimation is a well-known feature of DFT since it does not account for phonon scattering in the band structure [40]. In Fig. 15, the total and partial density of state (TDOS and PDOS) for the band configurations depicted in Fig. 14 are also shown. Because they provide information on hybridization and the orbital character of the states, the PDOS are extremely valuable.

The substitution of Ga by Al causes an increase in the band gap due to

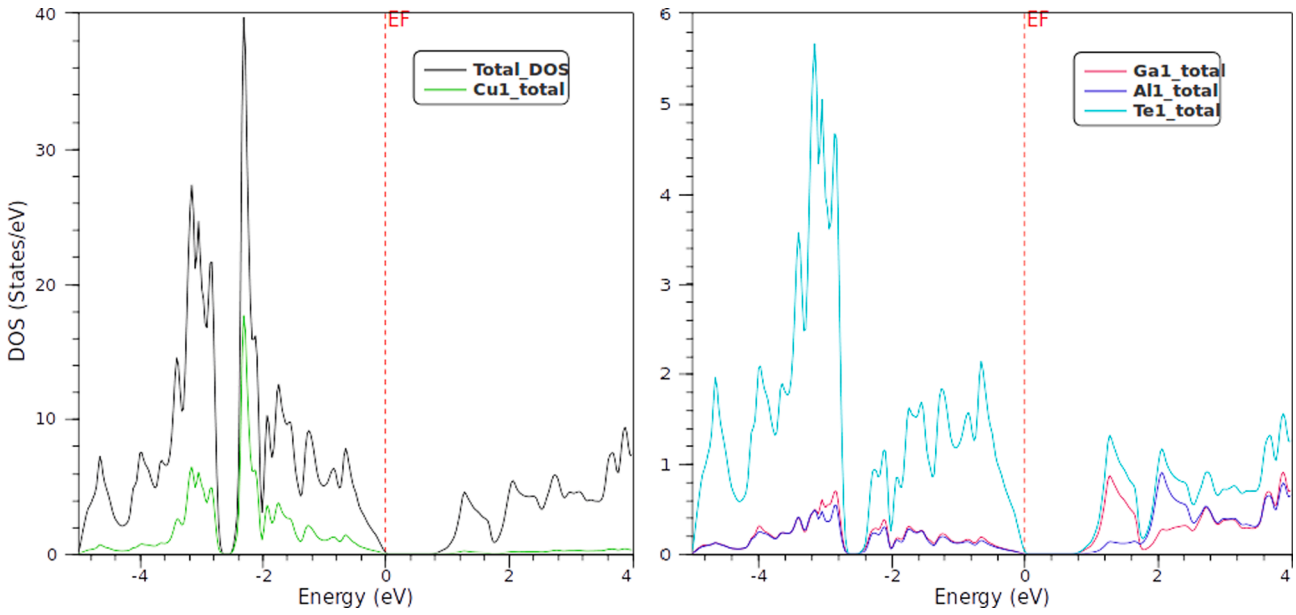

Fig. 13. Total and partial density of states for $CuAl_{0.5}Ga_{0.5}Te_2$.

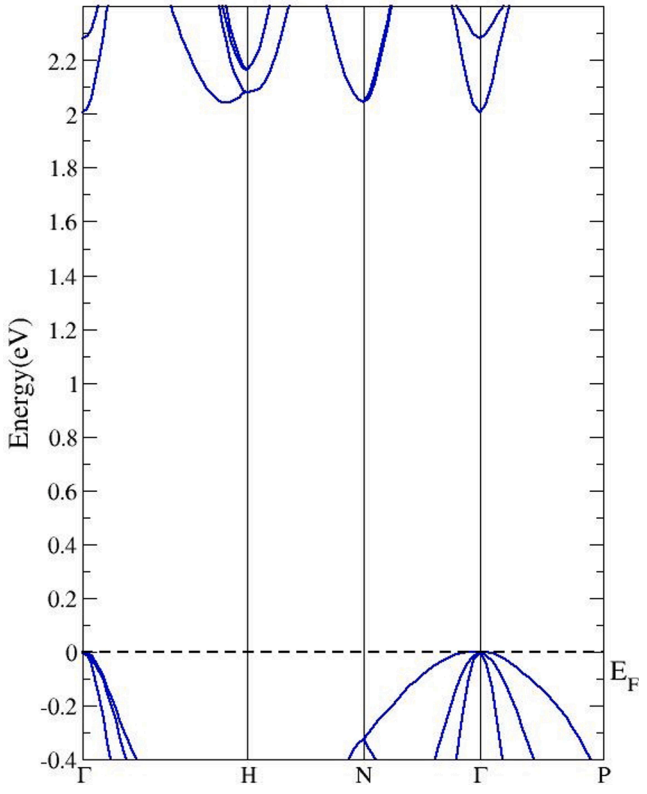

Fig. 14. Energy band structure of $CuAlTe_2$ using mBJ.

a decrease in the VBM due to the large contribution of the Al-s state and a modest rise in the CBM from the Fermi energy level due to the contribution of the Al-s state. In addition, the energy band gap widens due to the difference in electronegativity between Al and Ga [41]. The Al-s and Te-p states dominate the region of the conduction band between 1.5 and 2 eV, with the Al-s states having a substantial contribution and the Te-p states having a weak contribution.

4. Conclusions

$CuAl_xGa_{1-x}Te_2$ thin films were obtained by vacuum evaporation of mechanically alloyed powders. XRD analysis of the $CuAl_xGa_{1-x}Te_2$ powders and their deposit confirmed the chalcopyrite structure with a preferred orientation (1 1 2). The lattice parameters decreased linearly as the Al content increased, and the (1 1 2) peak diffraction shifted to a higher angle when the Ga atoms were replaced by the smaller Al atoms. According to the XPS study, the inserted Al atoms effectively replaced the Ga atoms in the $CuAl_xGa_{1-x}Te_2$ lattice. However, all of the deposited films had a high absorption coefficient in the visible range, indicating their applicability for solar cell applications. With increasing Al concentration, the optical band gap of the deposited films widened. The $CuAl_{0.5}Ga_{0.5}Te_2$ film, on the other hand, has a direct band gap of approximately 1.65 eV, which is near to the optimal band gap for the best photovoltaic conversion. The investigation of the electronic band structure of the compounds using ab initio calculations revealed that the band gap increases as the Al concentration increases, which are compatible with the experimental results. Furthermore, the direct band gaps of $CuGaTe_2$ and $CuAlTe_2$ were 1.073 and 2.0 eV, respectively. $CuAl_{0.5}Ga_{0.5}Te_2$, on the other hand, had an indirect band gap of 1.24 eV. All of the estimated band gap values were found to be lower than the experimental values; this is a well-known property of the DFT.

5. Data availability

The data that support the findings of this study are available from the corresponding author upon reasonable request.

Declaration of Competing Interest

The authors declare that they have no known competing financial interests or personal relationships that could have appeared to influence the work reported in this paper.

Data availability

No data was used for the research described in the article.

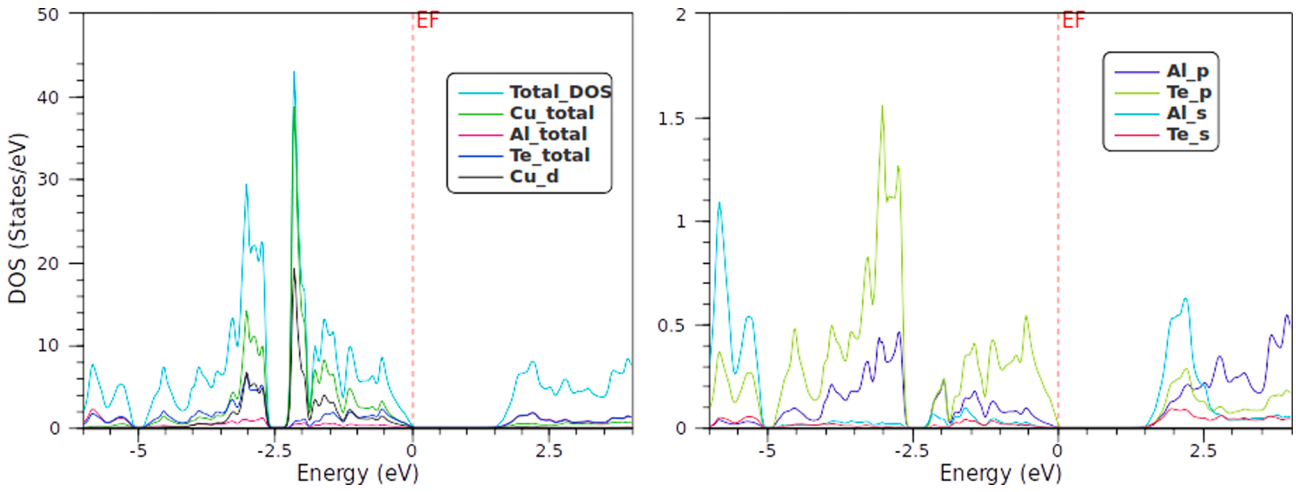

Fig. 15. Total and partial density of states for $CuAlTe_2$.

References

[1] J. Castro, J. Naranjo, L. Duran, L. Melendez, J.R. Fermin, J. Cendros, C.A. D. Rincón, Growth, structure and thermal properties of $CuAl_xGa_{1-x}Se_2$ alloys, Cryst. Res. Technol. J. Exp. Ind. Crystallogr. 41 (2006) 946–949, https://doi.org/10.1002/crat.200610702.

[2] K.W. Cheng, M.S. Fan, Preparation and characterization of $CuIn_xAl_{1-x}S_2$ films using the sulfurization of metal precursors for photoelectrochemical applications, J. Taiwan Inst. Chem. Eng. 44 (2013) 407–414, https://doi.org/10.1016/j.jtice.2012.12.013.

[3] C. Frisk, C. Platzer-Björkman, J. Olsson, P. Szaniawski, J.T. Wätjen, V. Fjällström, P. Salomé, M. Edoff, Optimizing Ga-profiles for highly efficient Cu(In, Ga)S_e2 thin film solar cells in simple and complex defect models, J. Phys. D. Appl. Phys. 47 (2014), 485104, https://doi.org/10.1088/0022-3727/47/48/485104.

[4] K.G. Deepa, N.L. Shruthi, M.A. Sunil, J. Nagaraju, Cu(In, Al)S_e2 thin films by one-step electrodeposition for photovoltaics, Thin Solid Films. 551 (2014) 1–7, https://doi.org/10.1016/j.tsf.2013.10.180.

[5] S.N. Malik, S. Mahboob, N. Haider, M.A. Malik, P. O'Brien, A colloidal synthesis of $CuInSe_2$, $CuGaSe_2$ and $CuIn_{1-x}Ga_xSe_2$ nanoparticles from diisopropyldiselenophosphinatometal precursors, Nanoscale. 3 (2011) 5132–5139, https://doi.org/10.1039/C1NR10888C.

[6] Y.C. Chen, Y.P. Lin, T.E. Hsieh, M.W. Huang, Preparation of Cu(In, Ga)S_e2 nanoparticles via solvothermal method in conjunction with ball milling process and its applications to thin-film solar cells, J. Alloys Compd. 791 (2019) 1–10, https://doi.org/10.1016/j.jallcom.2019.03.253.

[7] M.I. Hussain, R.M.A. Khalil, F. Hussain, Computational exploration of structural, electronic, and optical properties of novel combinations of inorganic ruddlesden–popper layered perovskites Bi2XO4 (X= Be, Mg) using tran and blaha-modified becke–johnson approach for optoelectronic applications, Energy Technol. 9 (2021) 2001026, https://doi.org/10.1002/ente.202001026.

[8] S. Hayat, R.M.A. Khalil, M.I. Hussain, A.M. Rana, F. Hussain, A DFT study of perovskite type halides KBeBr 3, RbBeBr3, and CsBeBr3 in triclinic phase for advanced optoelectronic devices, Solid State Commun. 344 (2022), 114674, https://doi.org/10.1016/j.ssc.2022.114674.

[9] P. Cheng, T. Wu, Y. Li, L. Jiang, W. Deng, K. Han, Combining theory and experiment in the design of a lead-free ((CH 3 NH 3) 2 AgBiI 6) double perovskite, New J. Chem. 41 (2017) 9598–9601, https://doi.org/10.1039/C7NJ02365K.

[10] M.I. Hussain, R.M.A. Khalil, F. Hussain, M. Imran, A.M. Rana, S. Kim, Investigations of structural, electronic and optical properties of YInO3 (Y= Rb, Cs, Fr) perovskite oxides using mBJ approximation for optoelectronic applications: a first principles study, Mater. Sci. Semicond. Process. 113 (2020), 105064, https://doi.org/10.1016/j.mssp.2020.105064.

[11] R.W. Birkmire, Compound polycrystalline solar cells: Recent progress and Y2 K perspective, Sol. Energy Mater. Sol. Cells. 65 (2001) 17–28, https://doi.org/10.1016/S0927-0248(00)00073-8.

[12] M. Benabdeslem, H. Sehli, S. Rahal, N. Benslim, L. Bechiri, A. Djekoun, T. Touam, M. Boujnah, A. El Kenz, A. Benyoussef, X. Portier, Ab Initio Calculations and Experimental Properties of $CuAl_xGa_{1-x}Te_2$ for Photovoltaic Solar Cells, J. Electron. Mater. 45 (2) (2016) 1035–1040.

[13] H. Sehli, M. Benabdeslem, N. Benslim, L. Bechiri, H. Ayed, A. Djekoun, M. Boujnah, X. Portier, S. Ammar, H. Lecoq, Formation and Study of the Nanostructured CuAlGaTe Synthesized by Mechanical Alloying Processing, JOM J. Miner. Met. Mater. Soc. 66 (2014), https://doi.org/10.1007/s11837-014-0957-4.

[14] I.V. Bodnar, I.A. Victorov, V.M. Dabranski, Crystal growth and investigation of $CuAl_xGa_{1-x}Te_2$ solid solutions, J. Cryst. Growth. 265 (2004) 214–219, https://doi.org/10.1016/j.jcrysgro.2004.01.058.

[15] J.P. Perdew, K. Burke, M. Ernzerhof, Perdew, burke, and ernzerhof reply, Phys. Rev. Lett. 80 (1998) 891. https://doi.org/10.1103/PhysRevLett.80.891.

[16] E.A. Khera, H. Ullah, M. Imran, N.A. Niaz, F. Hussain, R.M.A. Khalil, U. Rasheed, M.A. Sattar, F. Iqbal, C. Mahta, Structural, electronic and optical properties of transition metal doped Hf1-xTMxO2 (TM= Co, Ni and Zn) using modified TB-mBJ potential for optoelectronic memristors devices, Optik (Stuttg). 212 (2020), 164677, https://doi.org/10.1016/j.ijleo.2020.164677.

[17] J.D. Pack, H.J. Monkhorst, Special points for Brillouin-zone integration - a reply, Phys. Rev. B. 16 (1977) 1748, https://doi.org/10.1103/PhysRevB.16.1748.

[18] Y.B.K. Reddy, V.S. Raja, B. Sreedhar, Growth and characterization of $CuIn_{1-x}Al_xSe_2$ thin films deposited by co-evaporation, J. Phys. D. Appl. Phys. 39 (2006) 5124, https://doi.org/10.1088/0022-3727/39/24/005.

[19] H. Cao, H. Deng, J. Tao, W. Zhou, X. Meng, L. Sun, P. Yang, J. Chu, Microstructural and morphological properties of sputtered Cu(In, Al)S_e2 thin films for solar cell applications, Mater. Lett. 157 (2015) 42–44, https://doi.org/10.1016/j.matlet.2015.05.021.

[20] E. Halgand, J.C. Bernede, S. Marsillac, J. Kessler, Physico-chemical characterisation of Cu(In, Al)S_e2 thin film for solar cells obtained by a selenisation process, Thin Solid Films. 480 (2005) 443–446, https://doi.org/10.1016/j.tsf.2004.11.039.

[21] K. Yılmaz, H. Karaagac, Annealing effects on structural, optical and electrical properties of e-beam evaporated $CuIn_{0.5}Ga_{0.5}Te_2$ thin films, Appl. Surf. Sci. 256 (21) (2010) 6454–6458.

[22] T. Plirdpring, K. Kurosaki, A. Kosuga, T. Day, S. Firdosy, V. Ravi, G.J. Snyder, A. Harnwunggmoung, T. Sugahara, Y. Ohishi, Chalcopyrite $CuGaTe_2$: a high efficiency bulk thermoelectric material, Adv. Mater. 24 (2012) 3622–3626, https://doi.org/10.1002/adma.201200732.

[23] A. Rivero, M. Quintero, C. Power, J. Gonzalez, R. Tovar, J. Ruiz, Temperature variation of optical energy gap values of the compound $CuGaTe_2$, J. Electron. Mater. 26 (1997) 1428–1432, https://doi.org/10.1007/s11664-997-0062-3.

[24] J. Shen, X. Zhang, Z. Chen, S. Lin, J. Li, W. Li, S. Li, Y. Chen, Y. Pei, Substitutional defects enhancing thermoelectric $CuGaTe_2$, J. Mater. Chem. A. 5 (2017) 5314–5320, https://doi.org/10.1039/C6TA10770B.

[25] H.J. Al-Asedy, S.A. Al-Khafaji, H. Bakhtiar, N. Bidin, Properties of Al-and Ga-doped thin zinc oxide films treated with UV laser radiation, Appl. Phys. A. 124 (2018) 1–12, https://doi.org/10.1007/s00339-018-1619-0.

[26] J. López-García, C. Guillén, $CuIn_{1-x}Al_xSe_2$ thin films obtained by selenization of evaporated metallic precursor layers, Thin Solid Films. 517 (2009) 2240–2243, https://doi.org/10.1016/j.tsf.2008.10.095.

[27] J. Shewchun, J. Loferski, R. Beaulieu, G.H. Chapman, B.K. Garside, A/sup I//sub 1-y/B/sup I//sub y/C/sup III/D/sup VI//sub 2x/E/sup VI//sub (21–x/) pentenary alloy system and its application to photovoltaic solar energy conversion, J. Appl. Phys.; (United States) 50 (1979), https://doi.org/10.1063/1.325854.

[28] J. Castro, J. Naranjo, L. Durán, L. Meléndez, J.R. Fermin, J. Cendros, C.A. D. Rincón, Growth, structure and thermal properties of $CuAl_xGa_{1-x}Se_2$ alloys, Cryst. Res. Technol. 41 (2006) 946–949, https://doi.org/10.1002/crat.200610702.

[29] U. Parihar, K. Sreenivas, J.R. Ray, C.J. Panchal, N. Padha, B. Rehani, Influence of substrate temperature on structural, optical, and electrical properties of flash evaporated $CuIn_{0.81}Al_{0.19}Se_2$ thin films, Mater. Chem. Phys. 139 (2013) 270–275, https://doi.org/10.1016/j.matchemphys.2013.01.034.

[30] J. López-García, C. Guillén, J. Herrero, Influence of the annealing temperature on $CuAl_xGa_{1-x}Se_2$ thin films obtained by selenization, Phys. Status Solidi. 209 (2012) 1467–1474, https://doi.org/10.1002/pssa.201228017.

[31] A. Shaukat, Composition-dependent band gap variation of mixed chalcopyrites, J. Phys. Chem. Solids. 51 (1990) 1413–1418, https://doi.org/10.1016/0022-3697(90)90024-A.

[32] P. Guha, S. Roy, S. Chaudhuri, A.K. Pal, Synthesis and characterization of $CuGaTe_2$ films prepared by three source co-evaporation technique, J. Phys. D. Appl. Phys. 35 (2002) 1504, https://doi.org/10.1088/0022-3727/35/13/309.

[33] K.V. Reddy, J.L. Annapurna, Optical absorption and electrical conductivity of flash evaporated $CuGaTe_2$ thin films, Pramana. 26 (1986) 269–276, https://doi.org/10.1007/BF02845267.
[34] M.S. Reddy, K.T.R. Reddy, O.M. Hussain, P.J. Reddy, Investigations on polycrystalline $CuGaTe_2$ thin films, Thin Solid Films. 292 (1997) 14–19, https://doi.org/10.1016/S0040-6090(96)08950-X.
[35] I.V. Bodnar, V.F. Gremenok, I.A. Viktorov, D.D. Krivolap, Investigation of the properties of $CuGaTe_2$ thin films, Tech. Phys. Lett. 24 (1998) 89–90, https://doi.org/10.1134/1.1262007.
[36] V.K. Gudelli, V. Kanchana, G. Vaitheeswaran, $CuAlTe_2$: A promising bulk thermoelectric material, J. Alloys Compd. 648 (2015) 958–965, https://doi.org/10.1016/j.jallcom.2015.07.042.
[37] W. Feng, D. Xiao, Y. Zhang, Y. Yao, Half-Heusler topological insulators: A first-principles study with the Tran-Blaha modified Becke-Johnson density functional, Phys. Rev. B. 82 (2010), 235121, https://doi.org/10.1103/PhysRevB.82.235121.
[38] F. Tran, P. Blaha, Accurate band gaps of semiconductors and insulators with a semilocal exchange-correlation potential, Phys. Rev. Lett. 102 (2009) 5–8, https://doi.org/10.1103/PhysRevLett.102.226401.
[39] I.V. Bodnar, $CuGaTe_2$–$CuAlTe_2$ System, Inorg. Mater. 39 (2003) 10–14.
[40] X.D. Chen, L. Chen, Q.Q. Sun, P. Zhou, D.W. Zhang, Hybrid density functional theory study of $Cu(In_{1-x}Ga_x)Se_2$ band structure for solar cell application, AIP Adv. 4 (2014), https://doi.org/10.1063/1.4893238.
[41] C.S. Schnohr, Compound semiconductor alloys: From atomic-scale structure to bandgap bowing, Appl. Phys. Rev. 2 (2015) 31304, https://doi.org/10.1063/1.4930002.